JOURNAL OF COMPUTATIONAL PHYSICS **144,** 213–234 (1998)
ARTICLE NO. CP985997

# Perfectly Matched Layer as an Absorbing Boundary Condition for the Linearized Euler Equations in Open and Ducted Domains

Christopher K. W. Tam,* Laurent Auriault,* and Francesco Cambuli†

**Department of Mathematics, Florida State University, Tallahassee, Florida 32306-4510; and †Dipartimento di Ingegneria Meccanica, Universita degli Studi di Cagliari, Piazza d'Armi, 09123, Cagliari, Italy*
E-mail: tam@math.fsu.edu

Received October 30, 1997; revised April 6, 1998

Recently, perfectly matched layer (PML) as an absorbing boundary condition has found widespread applications. The idea was first introduced by Berenger for electromagnetic waves computations. In this paper, it is shown that the PML equations for the linearized Euler equations support unstable solutions when the mean flow has a component normal to the layer. To suppress such unstable solutions so as to render the PML concept useful for this class of problems, it is proposed that artificial selective damping terms be added to the discretized PML equations. It is demonstrated that with a proper choice of artificial mesh Reynolds number, the PML equations can be made stable. Numerical examples are provided to illustrate that the stabilized PML performs well as an absorbing boundary condition. In a ducted environment, the wave modes are dispersive. It will be shown that in the presence of a mean flow the group velocity and phase velocity of these modes can have opposite signs. This results in a band of transmitted waves in the PML to be spatially amplifying instead of evanescent. Thus in a confined environment, PML may not be suitable as an absorbing boundary condition unless there is no mean flow. 

## 1. INTRODUCTION

Recently, Berenger [1, 2] succeeded in formulating an absorbing boundary condition for computational electromagnetics that has the unusual characteristic that when an outgoing disturbance impinges on the interface between the computation domain and the absorbing layer surrounding it, no wave is reflected back into the computation domain. In other words, all the outgoing disturbances are transmitted into the absorbing layer where they are damped out. Such a layer has come to be known as a perfectly matched layer (PML).

Since its initial development, PML has found widespread applications in elastic wave propagation [3], computational aeroacoustics, and many other areas. Hu [4] was the first to



0021-9991/98 $25.00

apply PML to aeroacoustics problems governed by the linearized Euler equations, linearized over a uniform mean flow. He has since extended his work to nonuniform mean flow and for the fully nonlinear Euler equations [5]. Further applications of PML to acoustics problems including wavemodes in ducts can be found in the most recent works of Hu and co-workers [6, 7]. In these references, examples are provided that indicate that high quality numerical solutions could be found with PML used as radiation or outflow boundary conditions.

In open unbounded domains, acoustic waves are nondispersive and propagate with the speed of sound relative to the local mean flow. Inside a duct, the situation is completely different. Acoustic waves are repeatedly reflected back by the confining walls. For ducts with parallel walls, the continuous reflection of the acoustic waves by the wall leads to the formation of coherent wave patterns called duct modes [8, 9]. Unlike the open domain, duct modes are dispersive with phase and group velocities vary with axial wavenumber. Because of the dispersive nature of the duct modes many radiation boundary conditions that work well in open domains are known to be inappropriate for ducted environments. For this reason, Tam [10] in a recent review on numerical boundary conditions for computational aeroacoustics suggested that the boundary condition for a ducted environment be regarded as a category of its own.

There are three primary objectives in this work. First, we intend to show that in the presence of a mean flow normal to a PML, the standard PML equations of the linearized Euler equations support unstable solutions. Earlier Tam [10] pointed out that the PML equations with mean flow have unstable solutions. However, he did not show that the existence of instabilities is due to the mean flow component normal to the layer. The origin and characteristics of these instabilities are investigated and analyzed. It is interesting to mention that in his earliest work, Hu [4] reported that his computation encountered numerical instability. But by applying numerical filtering, he was able to obtain stable solutions. In light of our finding, we believe that what Hu encountered was not instability of his numerical scheme but that his numerical solution inadvertently excited the intrinsic unstable solution of the PML equations. Not directly related to the instability of the PML equations, Abarbanel and Gottlieb [11] recently analyzed the electromagnetic PML equations. They concluded that the equations are only weakly well-posed.

Second, we will show that the instability is not very strong, namely, the growth rates are small. Also the instabilities are confined primarily to short waves. It is, therefore, possible to suppress the instabilities by the addition of artificial selective damping terms [12] to the discretized PML equations. It is important to point out that artificial selective damping eliminates mainly the short waves and has negligible effect on the long or the physical waves. Thus the addition of these damping terms does not effect the perfectly matched conditions of the PML.

Third, we will show that a perfectly matched layer may not be suitable as an absorbing boundary condition for waves in a ducted flow environment. The major difference between acoustic waves in an open domain and acoustic waves inside a duct is that in an unbounded region acoustic waves are nondispersive whereas duct modes are dispersive. It will be shown that in the presence of a mean flow the group and phase velocity of the duct modes can have opposite signs. Because of this, a band of transmitted waves will actually grow spatially instead of being damped in the PML. In other words, the PML equations do not damp these wave modes as absorbing boundary condition ought to do. The exception is when there is no mean flow in the duct. In this special case, all the transmitted waves are spatially damped.

In Section 2, the use of PML for open domain problems is discussed. The stability of the PML governing equations is investigated. It will be shown that the addition of damping terms to form the PML equations can actually cause the vorticity and acoustic wave modes to become unstable. The splitting of the variables in formulating the PML equations leads to a higher order system of equations. This higher system supports extra solutions. These extra or spurious solutions are found to become unstable when the damping coefficient is large. Numerical examples are provided to illustrate the spread of the unstable solution from the PML back into the interior of the computation domain.

In Section 3, the effect of the addition of artificial selective damping terms to the discretized PML equations is investigated. It is shown that with an appropriate choice of mesh Reynolds number, the unstable solutions of the PML equations can be suppressed. Numerical examples are given to demonstrate the effectiveness of the modified PML as a radiation/outflow boundary condition.

Section 4 deals with the theory and application of PML to ducted internal flow problems. An eigenvalue analysis is carried out to show the existence of a band of frequency for which the PML exerts no damping on the acoustic duct modes. These wave modes actually would grow in amplitude as they propagate through the PML. Numerical results are provided to illustrate the existence of this kind of amplifying ducted acoustic modes.

## 2. OPEN DOMAIN PROBLEMS

Let us consider the use of PML as absorbing boundary condition for the solution of the linearized Euler equations (linearized over a uniform mean flow) in a two-dimensional open domain as shown in Fig. 1. We will use $\Delta x = \Delta y$ (the mesh size) as the length scale, $a_0$ (the sound speed) as the velocity scale, $\frac{\Delta x}{a_0}$ as the time scale, and $\rho_0 a_0^2$ (where $\rho_0$ is the

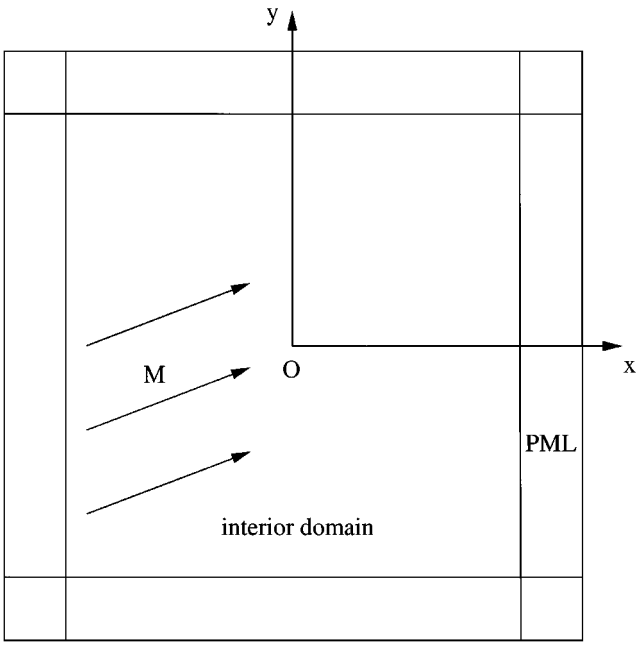


**FIG. 1.** Two dimensional computation domain with Perfectly Matched Layers as boundaries.

mean density) as the pressure scale. The dimensionless governing equations in the PML are formed by splitting the linearized Euler equations according to the spatial derivatives. An absorption term is added to each of the equations with spatial derivative in the direction normal to the layer. For example, for the PML on the right boundary of Fig. 1 (not at the corners) the governing equations are [4]

$$\begin{aligned}
\frac{\partial u_1}{\partial t} + \sigma u_1 + M_x \frac{\partial}{\partial x}(u_1 + u_2) + \frac{\partial}{\partial x}(p_1 + p_2) &= 0 \\
\frac{\partial u_2}{\partial t} + M_y \frac{\partial}{\partial y}(u_1 + u_2) &= 0 \\
\frac{\partial v_1}{\partial t} + \sigma v_1 + M_x \frac{\partial}{\partial x}(v_1 + v_2) &= 0 \\
\frac{\partial v_2}{\partial t} + M_y \frac{\partial}{\partial y}(v_1 + v_2) + \frac{\partial}{\partial y}(p_1 + p_2) &= 0 \\
\frac{\partial p_1}{\partial t} + \sigma p_1 + M_x \frac{\partial}{\partial x}(p_1 + p_2) + \frac{\partial}{\partial x}(u_1 + u_2) &= 0 \\
\frac{\partial p_2}{\partial t} + M_y \frac{\partial}{\partial y}(p_1 + p_2) + \frac{\partial}{\partial y}(v_1 + v_2) &= 0,
\end{aligned} \tag{1}$$

where $M_x$ and $M_y$ are the mean flow Mach numbers in the $x$ and $y$ directions. $\sigma$ is the absorption coefficient.

Suppose we look for solutions with $(x, y, t)$ dependence in the form $\exp[i(\alpha x + \beta y - \omega t)]$. It is easy to find from (1) that the dispersion relations of the PML equations are

$$\left(1 - \frac{\alpha M_x}{\omega + i\sigma} - \frac{\beta M_y}{\omega}\right)^2 - \frac{\alpha^2}{(\omega + i\sigma)^2} - \frac{\beta^2}{\omega^2} = 0 \tag{2}$$

$$1 - \frac{\alpha M_x}{\omega + i\sigma} - \frac{\beta M_y}{\omega} = 0. \tag{3}$$

In the limit $\sigma \to 0$, (2) and (3) become the well-known dispersion relations of the acoustic and the vorticity waves of the linearized Euler equations.

### 2.1. *Mean Flow Parallel to PML*

Dispersion relations (2) and (3) behave very differently depending on whether there is any mean flow normal to the PML. When the mean flow is parallel to the layer, i.e., $M_x = 0$, the solutions are stable. This is easy to see from (3) for the vorticity wave. Physically, if the mean flow is parallel to the PML, the vorticity waves in the computation domain, being convected by the mean flow, cannot enter the layer and hence would not lead to unstable solution.

To show that for $M_x = 0$ all the solutions of (2) are stable, a simple mapping will suffice. Rewrite (2) in the form

$$F \equiv (\omega - \beta M_y)^2 - \frac{\alpha^2 \omega^2}{(\omega + i\sigma)^2} = \beta^2. \tag{4}$$

Figure 2 shows the image of the upper-half $\omega$-plane in the $F$ plane. The upper-half $\omega$-plane is mapped into the entire $F$ plane except for the slit $ADC$. But since $\beta^2$ is real and positive,

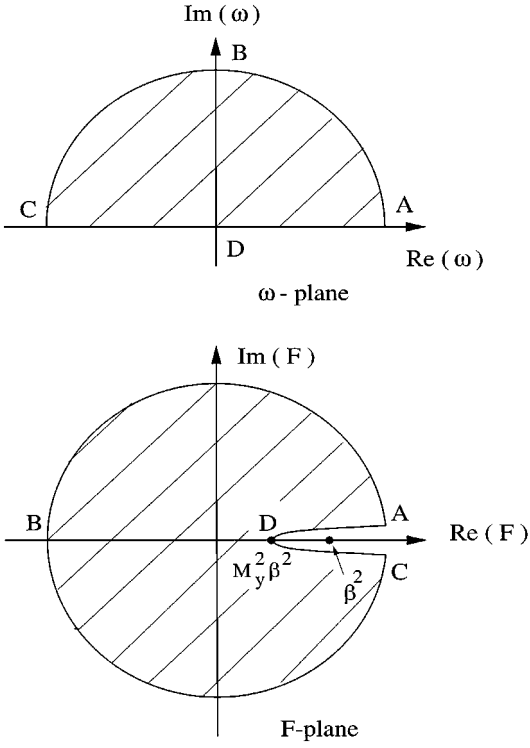


**FIG. 2.** The image of the upper half $\omega$-plane in the $F$-plane.

for subsonic mean flow the point $\beta^2$ lies outside the image. Thus no value of $\omega$ in the upper-half $\omega$-plane would satisfy Eq. (2) indicating that there is no unstable solution.

### 2.2. *Unstable Solutions of the PML Equations*

For $M_x \neq 0$, the PML equations support unstable solutions. It is to be noted that, unlike the original dispersion relation of the acoustic waves, Eq. (2) is a quadric equation in $\omega$. It has two extra roots in addition to the two modified acoustic modes. For small $\sigma$, the two spurious roots are damped but one of the modified acoustic roots is unstable. For larger $\sigma$, numerical solutions indicate that one of the spurious roots becomes unstable. In any case, the equation splitting procedure and the addition of an absorption term, both are vital to the suppression of reflections at the interface between the computation domain and the PML, inadvertently, lead to instabilities.

For small $\sigma$, the roots of (2) and (3) can be found by perturbation. Let

$$\omega^{(a)} = \omega_0^{(a)} + \sigma\omega_1^{(a)} + \sigma^2\omega_2^{(a)} + \cdots \tag{5}$$

$$\omega^{(v)} = \omega_0^{(v)} + \sigma\omega_1^{(v)} + \sigma^2\omega_2^{(v)} + \cdots, \tag{6}$$

where the roots of (2) and (3) are designated by a superscript $a$ (for acoustic waves) and $v$

(for vorticity waves). Substituting (5) and (6) into (2) and (3), it is straightforward to find

$$\omega_0^{(a)} = \omega_+, \qquad \omega_-, \qquad 0, \qquad 0 \tag{7}$$

where

$$\omega_\pm = (\alpha M_x + \beta M_y) \pm (\alpha^2 + \beta^2)^{\frac{1}{2}} \tag{8}$$

$$\omega_1^{(a)} = i\left[\frac{-\alpha^2 \mp \alpha M_x(\alpha^2+\beta^2)^{\frac{1}{2}}}{\alpha^2+\beta^2 \pm (\alpha M_x + \beta M_y)(\alpha^2+\beta^2)^{\frac{1}{2}}}\right] \tag{9}$$

$$\omega_0^{(v)} = \alpha M_x + \beta M_y, \qquad 0 \tag{9a}$$

$$\omega_1^{(v)} = \frac{-i}{1 + (M_y/M_x)(\beta/\alpha)}. \tag{9b}$$

Clearly if $\omega_1^{(a)}$ or $\omega_1^{(v)}$ has a positive imaginary part, the mode is unstable. It is easy to show, especially in the case $M_y = 0$, that there are always values of $\alpha$ and $\beta$ such that $\omega_1^{(a)}$ of (9) is purely imaginary and positive. Similarly, from (9b) for $\frac{\beta}{\alpha} < 0$ and $|\frac{\beta}{\alpha}| > \frac{M_x}{M_y}$, $\omega_1^{(v)}$ is also purely positive imaginary. Thus the PML equations in the presence of a uniform flow with $M_x \neq 0$ support unstable solutions.

The unstable solutions of dispersion relations (2) and (3) can also be found numerically. For a given $(\alpha, \beta)$ the growth rates, $\omega_i$, of the unstable solutions can be calculated in a straightforward manner. Figure 3 shows the $\omega_i$ contours of the most unstable solution of Eq. (2), the acoustic mode, in the $\alpha - \beta$-plane for the case $M_x = 0.3$, $M_y = 0.0$, and $\sigma = 1.5$. Figure 4 shows a similar plot for the vorticity wave mode (Eq. (3)). In these figures only the unstable regions are shown. It is clear that there are instability waves over a wide range of wavenumbers. Numerical results indicate that, in general, the unstable regions expand as the flow Mach number or the damping coefficient $\sigma$ increases.

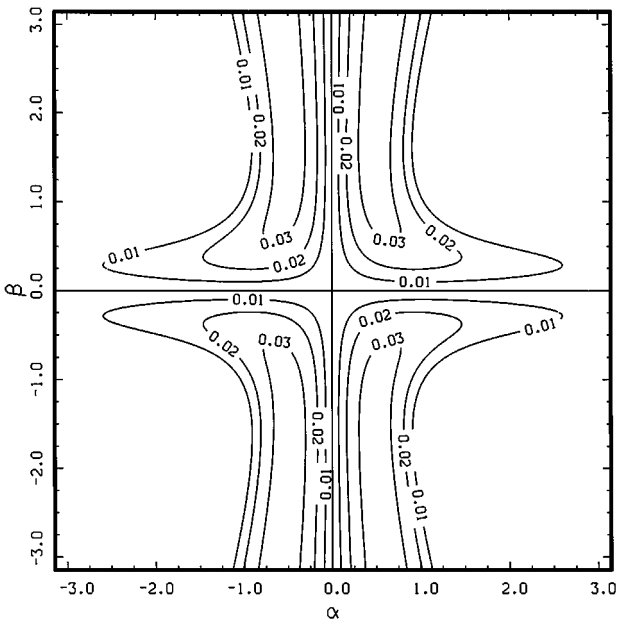


**FIG. 3.** Contours of the growth rate of the most unstable wave (acoustic mode) in the $\alpha - \beta$ plane. $M_x = 0.3$, $M_y = 0.0$, $\sigma = 1.5$.

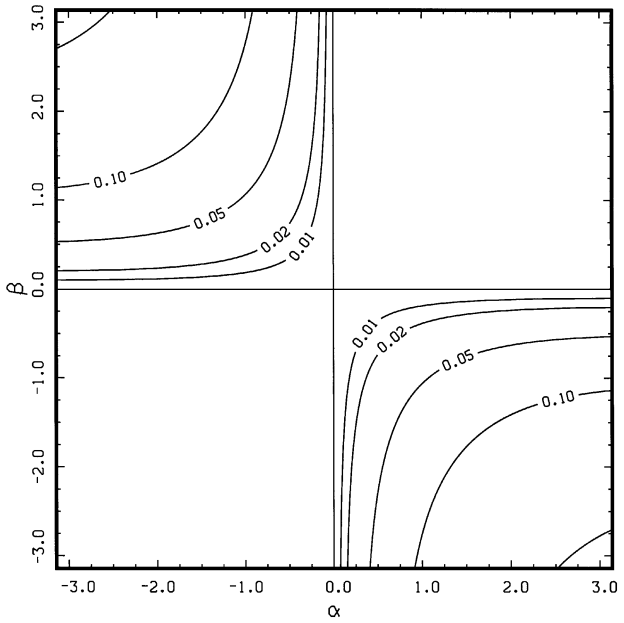


**FIG. 4.** Contours of the growth rate of the most unstable vorticity wave in the $\alpha - \beta$ plane. $M_x = 0.3$, $M_y = 0.2$, $\sigma = 1.0$.

### 2.3. *Numerical Examples*

The nature and characteristics of the unstable waves associated with the acoustic mode and the vorticity mode are quite different. To illustrate the excitation of these unstable solutions in the PML by disturbances propagating or convecting from the interior computation domain, a series of numerical experiments has been carried out. Figure 5 shows the results of the case of a vorticity pulse convected into the PML when $M_x = 0.3$, $M_y = 0.2$, and $\sigma = 1.0$. The initial conditions for the pulse are (same as the initial conditions used by Tam and Webb [13])

$$\begin{aligned} p &= \rho = 0 \\ u &= 0.04y \exp\left[-(ln\,2)\left(\frac{x^2+y^2}{25}\right)\right] \\ v &= -0.04x \exp\left[-(ln\,2)\left(\frac{x^2+y^2}{25}\right)\right]. \end{aligned} \tag{10}$$

The DRP time marching scheme [13] is used in the simulation. The PML region extends from $x = 20$ to the right boundary of the computation domain. At the outermost boundary, the boundary condition $p_1 = p_2 = \rho_1 = \rho_2 = u_1 = u_2 = v_1 = v_2 = 0$ is imposed. Plotted in Fig. 5 are contours of the $u$ velocity component. Figure 5a shows the initial profile of the contours at $t = 0$. Figure 5b, at $t = 50$, reveals that there is damping of the vorticity pulse as it begins to enter the PML. This damping is the result of the built-in damping, $\sigma$, of the PML. Figure 5c, at a later time $t = 90$, shows the growth of the excited unstable solution in the PML. Finally, Fig. 5d (at $t = 130$) shows the spread of the unstable solution back into the interior computation domain. Figure 6 gives the corresponding waveform of the vorticity wave pulse. Figure 6d clearly indicates that the spread of the unstable vorticity waves in the PML can quickly contaminate the entire computation domain.

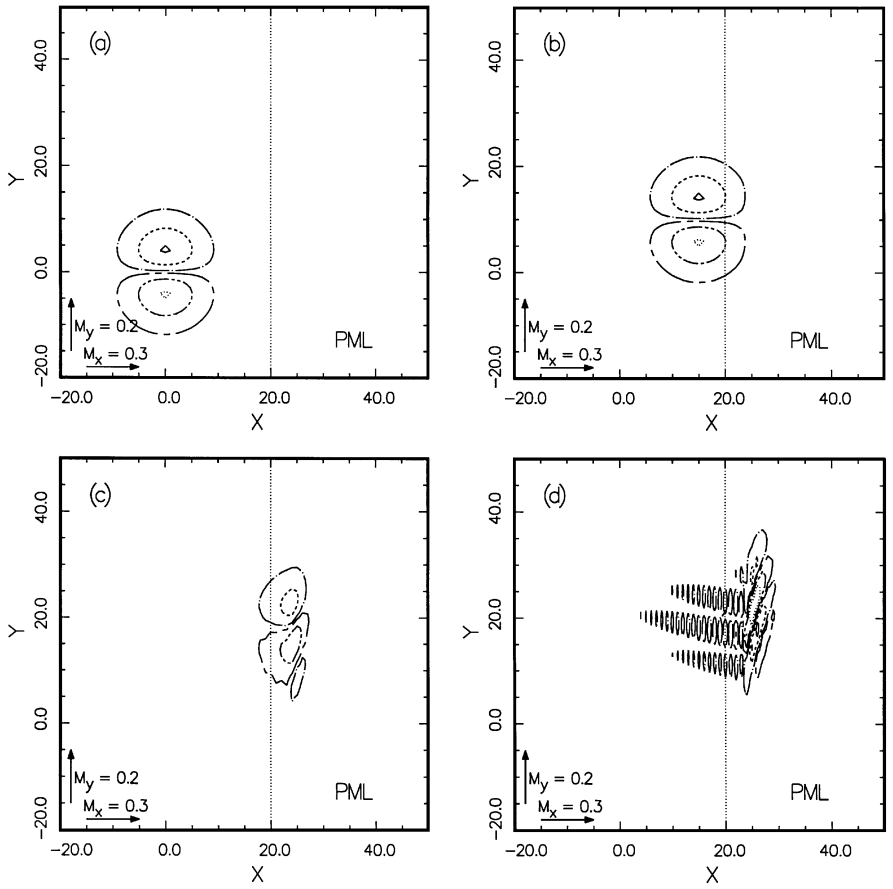


**FIG. 5.** Numerical simulation showing the generation and propagation of unstable vorticity-mode waves in the PML. $M_x = 0.3$, $M_y = 0.2$, $\sigma_m = 1.0$. (a) $t = 0$, (b) $t = 50$, (c) $t = 90$, (d) $t = 130$. Contours of the $u$ velocity component. —, 0.1; - -, 0.05; —·—, 0.01; — - —, −0.01; - - —, −0.05; · · · , −0.1.

Figures 7 and 8 are similar plots illustrating the excitation of the acoustic mode unstable solution in the PML. The Mach number and damping coefficient are $M_x = 0.5$, $M_y = 0.0$, and $\sigma = 1.5$. The initial disturbance consists of a pressure pulse given by

$$p = \rho = \exp\left[-(ln\,2)\left(\frac{x^2 + y^2}{9}\right)\right] \qquad (11)$$
$$u = v = 0.$$

The acoustic pulse generated by the initial disturbance propagates at a speed equal to the sound speed plus the flow velocity. Thus, the pulse leaves the small interior computation domain ($50 \times 50$) very quickly. Figure 7a shows the pressure contours at $t = 140$. At this time, the acoustic pulse is gone. The contours are associated with the excited unstable waves of the acoustic mode. These unstable waves move at a slow speed. Figure 7b is at $t = 200$. On comparing Figs. 7a and 7b, it is evident that there is significant growth of the unstable waves. Upon reaching the outermost boundary of the computation domain the unstable waves are reflected back as short waves. This is illustrated in Fig. 7c. The reflected short waves propagate at ultrafast speed. They contaminate the computation domain in a short period

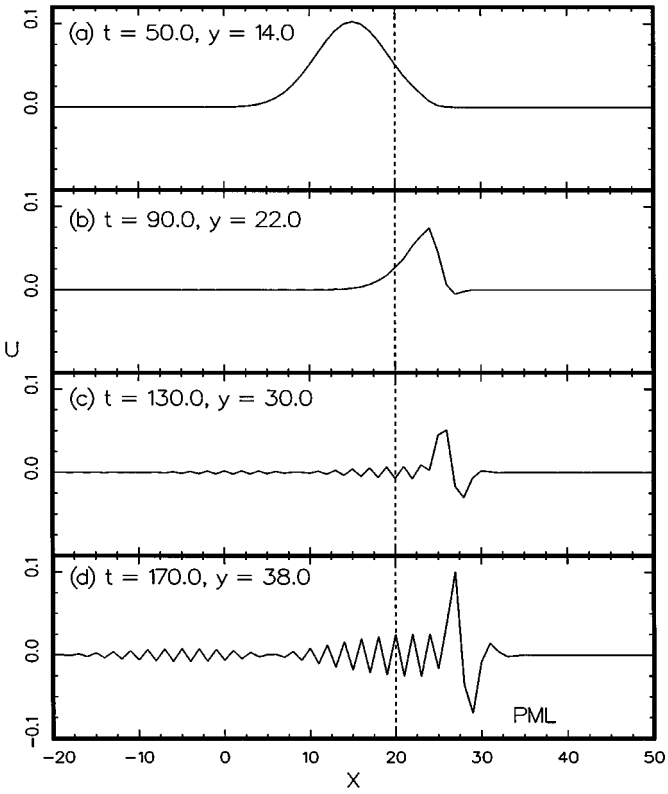


**FIG. 6.** Waveforms of $u$ showing the generation of unstable vorticity-mode waves excited by vorticity waves convected from the interior computation domain to the PML and the subsequent contamination of the interior computation domain. $M_x = 0.3$, $M_y = 0.2$, $\sigma_m = 1.0$.

of time as shown in Fig. 7d. Figure 8 shows the growth of the pressure waveform of the unstable acoustic mode waves in the PML before they reach the outer boundary of the computation domain. The measured growth rate of the most unstable wave has been found to agree with that calculated by the dispersion relation.

## 3. DEVELOPMENT OF A STABLE PML

### 3.1. *Artificial Selective Damping*

To ensure practicality, the thickness of a PML would normally be limited to around 15 to 20 mesh spacings. For a PML with such a thickness, it is easy to show that if the transmitted wave from the computation domain is to be reduced by a factor of $10^5$ in the presence of a subsonic mean flow, the damping coefficient $\sigma$ of (1) should have a value of about 1.5. By solving the dispersion relations (2) and (3) numerically, it has been found that for $\sigma = 1.5$ the unstable wave solutions have only a modest rate of growth. Moreover, these waves, generally, have short wavelengths. Mild instabilities of this type can be effectively suppressed by the addition of artificial selective damping terms [12, 14] to the discretized governing equations. The advantage of using artificial selective damping is that the damping is confined primarily to short waves. Thus, the perfectly matched condition is not adversely affected for the long waves (the physical waves) of the computation.

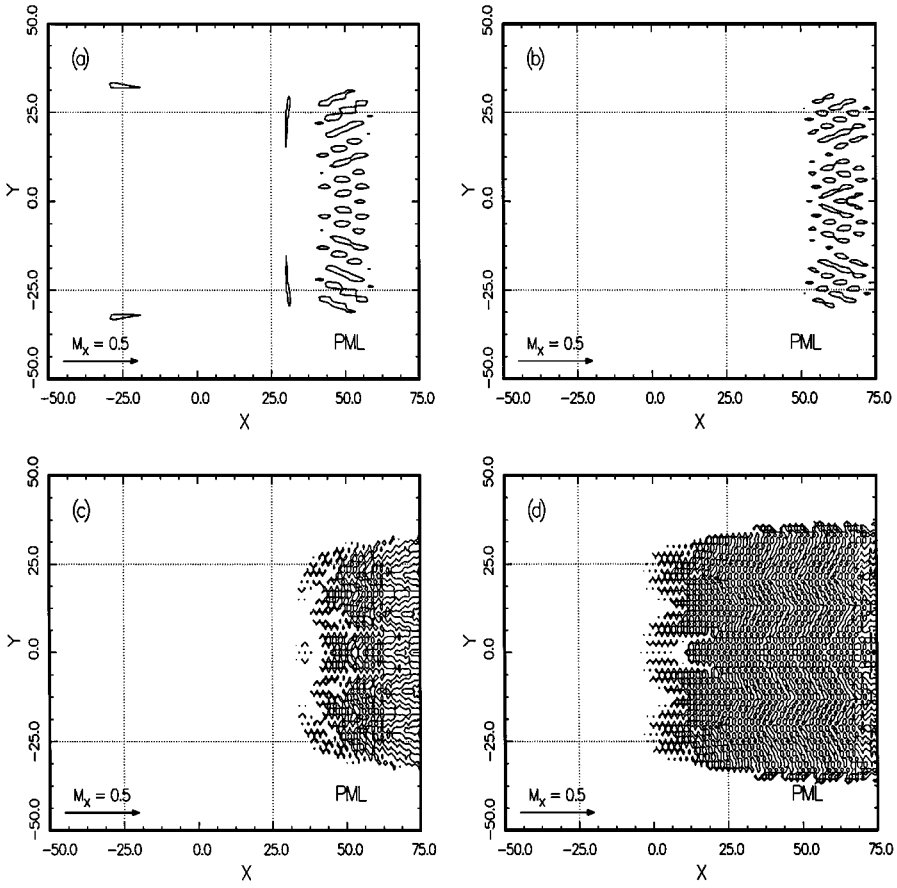


**FIG. 7.** Numerical simulation showing the generation and propagation of unstable acoustic-mode waves in the PML. $M_x = 0.5$, $M_y = 0.0$, $\sigma_m = 1.5$. Contours of pressure. (a) $t = 140$, $—p = 10^{-4}$; (b) $t = 200$, $—p = 5.10^{-3}$; (c) $t = 260$, $—p = 5.10^{-2}$; (d) $t = 300$, $—p = 5.10^{-2}$.

Consider the first equation of (1). Let $(l, m)$ be the spatial indices in the $x$- and $y$-directions. The semi-discretized form of this equation using the DRP scheme with artificial selective damping terms added to the right side is

$$\frac{d}{dt}(u_1)_{l,m} + \sigma(u_1)_{l,m} + \sum_{j=-3}^{3} a_j[M_x(u_1+u_2)_{l+j,m} + (p_1+p_2)_{l+j,m}]$$
$$= -\frac{1}{R_\Delta}\sum_{j=-3}^{3} d_j[(u_1)_{l+j,m} + (u_1)_{l,j+m}], \tag{12}$$

where $d_j$'s are the artificial selective damping coefficients [14] and $R_\Delta = a_\infty \frac{\Delta x}{\nu_a}$ is the artificial mesh Reynolds number. Terms similar to those on the right side of (12) are to be added to all the other discretized equations.

For the purpose of suppressing unstable solutions in the PML, we recommend the use of a damping curve with a slightly larger half-width then those given in Ref. [14]. In this

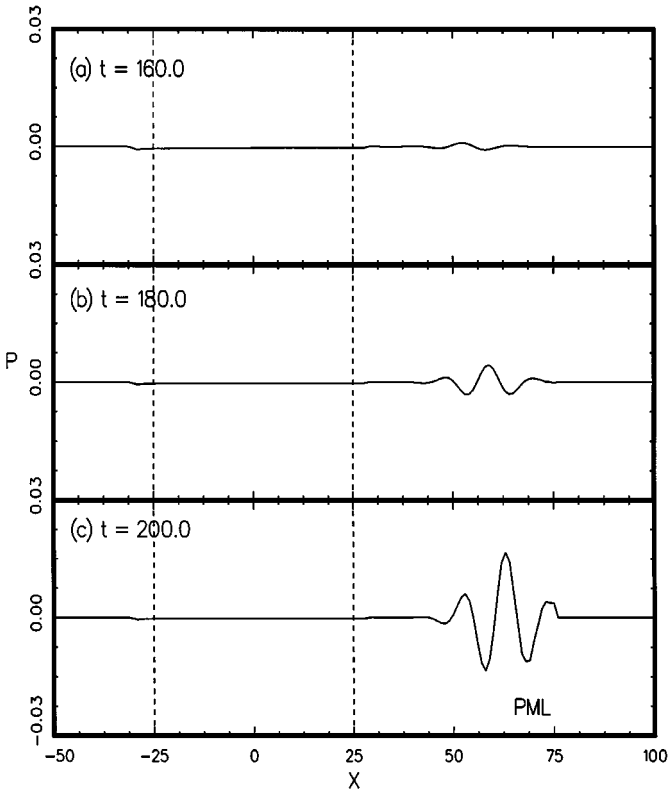


**FIG. 8.** Waveforms of pressure along $y = 0$ showing the generation of unstable acoustic-mode waves in the PML excited by acoustic disturbances from the computation domain. $M_x = 0.5$, $M_y = 0.0$, $\sigma_m = 1.5$.

work, the following damping coefficients (half-width $= 0.35\pi$) are used:

$$\begin{aligned} d_0 &= 0.3705630354 \\ d_1 = d_{-1} &= -0.2411788110 \\ d_2 = d_{-2} &= 0.0647184823 \\ d_3 = d_{-3} &= -0.0088211899. \end{aligned} \tag{13}$$

The damping rate of the artificial selective damping terms can be found by taking the Fourier transform of the right side of (12) (see [12]). Let $(\alpha, \beta)$ be the transform variables in the $(x, y)$-plane. The rate of damping for wavenumber $(\alpha, \beta)$ is

$$\text{damping rate} = \frac{1}{R_\Delta} D(\alpha, \beta), \tag{14}$$

where

$$D(\alpha, \beta) = \sum_{j=-3}^{3} d_j (e^{ij\alpha} + e^{ij\beta}). \tag{15}$$

Contours of the damping function $D(\alpha, \beta)$ in the $\alpha - \beta$-plane are shown in Fig. 9.

To demonstrate that suppression of the unstable solutions can be achieved by adding artificial selective damping terms to the discretized form of Eq. (1), let us consider the

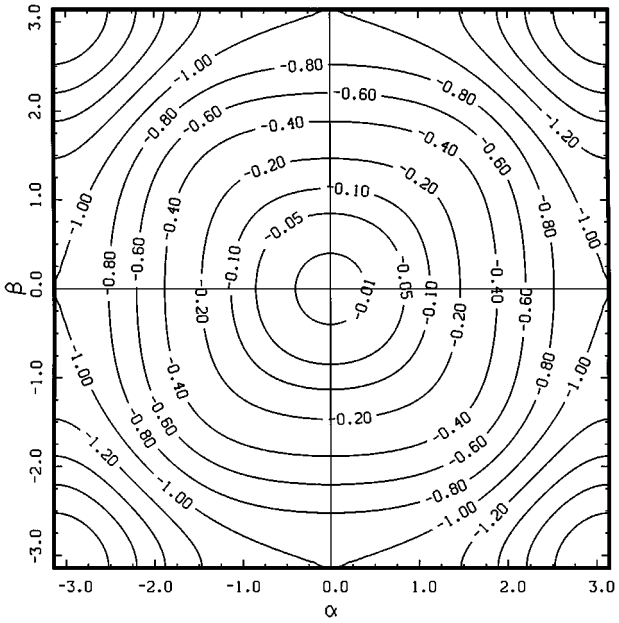


**FIG. 9.** Contours of constant $D(\alpha, \beta)$ in the $\alpha - \beta$ plane. Damping coefficients $d_j$'s are given by (13).

unstable solution with growth rate given by Fig. 3. On combining the growth rate of Fig. 3 and the damping rate of Fig. 9 with $R_\Delta = 1.421$, the resulting growth contours, $(\mathrm{Im}(\omega) - D(\alpha, \beta)/R_\Delta)$, are shown in Fig. 10. Outside the dotted lines (wavenumbers inside the vertical dotted lines correspond to wavelengths too long to fit into a 15 mesh spacing PML)

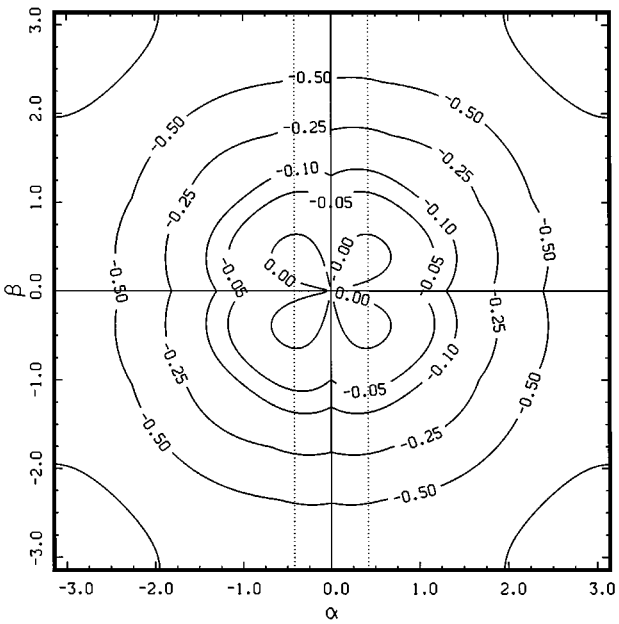


**FIG. 10.** Contours of combined growth and damping rates. $M_x = 0.3$, $M_y = 0.0$, $\sigma = 1.5$, $R_\Delta = 1.42$. Damping coefficients $d_j$'s are given by (13).

the combined effects result in damping of the waves. Thus all the instabilities of the PML equations are effectively suppressed.

### 3.2. *Distributions of $\sigma$ and $R_\Delta^{-1}$ in the PML*

In the implementation of PML as an absorbing boundary condition, Hu [4] suggested letting $\sigma$ vary spatially in the form

$$\sigma = \sigma_m \left( \frac{d}{D} \right)^{\lambda}, \tag{16}$$

where $D$ is the thickness of the PML, $d$ is the distance from the interface with the interior domain, and $\lambda$ is a constant. With the inclusion of artificial selective damping, we have found that the use of a well-designed smooth distribution of $\sigma$ and $R_\Delta^{-1}$ at the interface region is important if the perfectly matched condition is to be maintained in the finite difference form of the system of equations.

Figure 11 shows a distribution of $\sigma$ and $R_\Delta^{-1}$ we found to work well with the 7-point stencil DRP scheme. The $R_\Delta^{-1}$ curve is zero for the first two mesh points closest to the interface. It attends its full value $(R_\Delta^{-1})_{\max}$ at the 6th mesh point. A cubic spline curve is used in the transition region. With this arrangement, the first point where artificial damping occurs is the third point from the interface. This allows the use of the 7-point symmetric damping stencil in the PML except the last three points at the outer boundary. For these points, the 5-point and the 3-point stencil [14] should be used instead.

The $\sigma$ curve begins with the value $\sigma = 0$ at the fifth mesh point from the interface. The full value $\sigma_{\max}$ is reached at 8 mesh points further away. Again, a cubic spline curve is used in the transition region. The choice of starting the $\sigma$ curve at the fifth point is to ensure that the $R_\Delta^{-1}$ curve has attained its full value when $\sigma$ becomes nonzero.

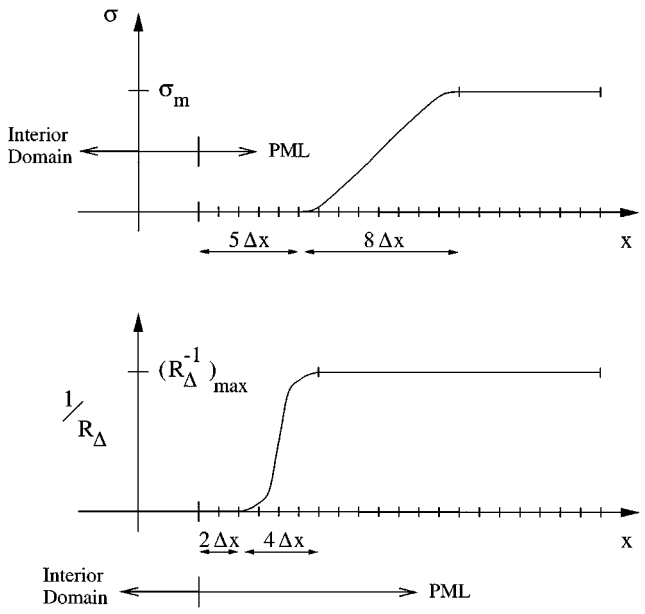


**FIG. 11.** Distributions of $\sigma$ and $R_\Delta^{-1}$ in a 20 mesh spacings PML.

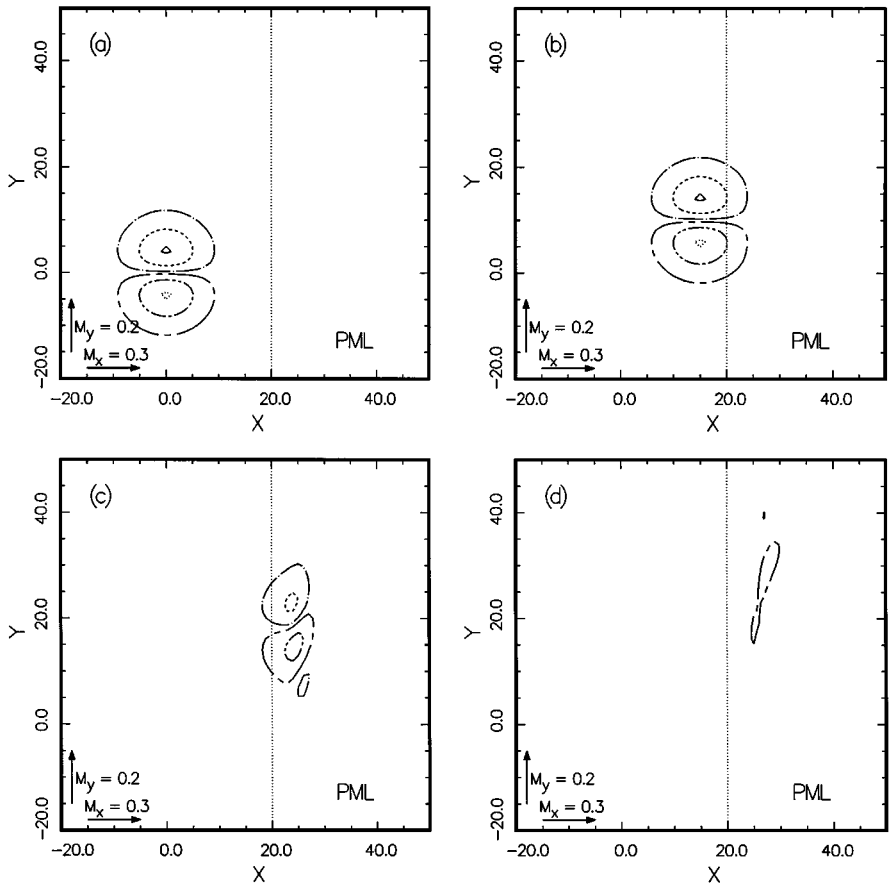


**FIG. 12.** Damping of a vorticity wave packet in the PML including artificial selective damping terms. $M_x = 0.3$, $M_y = 0.2$, $\sigma_m = 1.0$, $(R_\Delta^{-1})_{max} = 1.0$. (a) $t = 0$, (b) $t = 50$, (c) $t = 90$, (d) $t = 170$. Contours of the $u$ velocity component. —, 0.1; - -, 0.05; —·—, 0.01; — · —, −0.01; - - —, −0.05; · · · , −0.1.

### 3.3. *Numerical Examples*

To demonstrate the effectiveness of using artificial selective damping terms to suppress the instabilities of the PML equations, the numerical examples of Subsection 2.3 are reconsidered here. Artificial damping is now included in the simulations. Figure 12 shows the $u$-contours of the vorticity waves ($M_x = 0.3$, $M_y = 0.2$, $\sigma_m = 1.0$, $(R_\Delta^{-1})_{\max} = 1.0$) as they are convected from the interior domain to the PML. The vorticity wave packet is steadily damped. No sign of unstable waves of the type shown in Fig. 5 is detected. Figure 13 shows the corresponding waveform of $u$ at a few selected times. It is clear that the pulse is damped continuously once it propagates into the PML. The case of the acoustic disturbance has also been repeated with similar results. Based on these findings, it is concluded that a stable PML can be developed by the inclusion of artificial selective damping. Such a PML performs very effectively as an absorbing boundary condition in an open domain.

## 4. PML IN DUCTED ENVIRONMENTS

We will now consider the use of PML inside a circular duct of radius $R$. Dimensionless variables with respect to length scale $R$, velocity scale $a_t$ (speed of sound at $r = R$), time

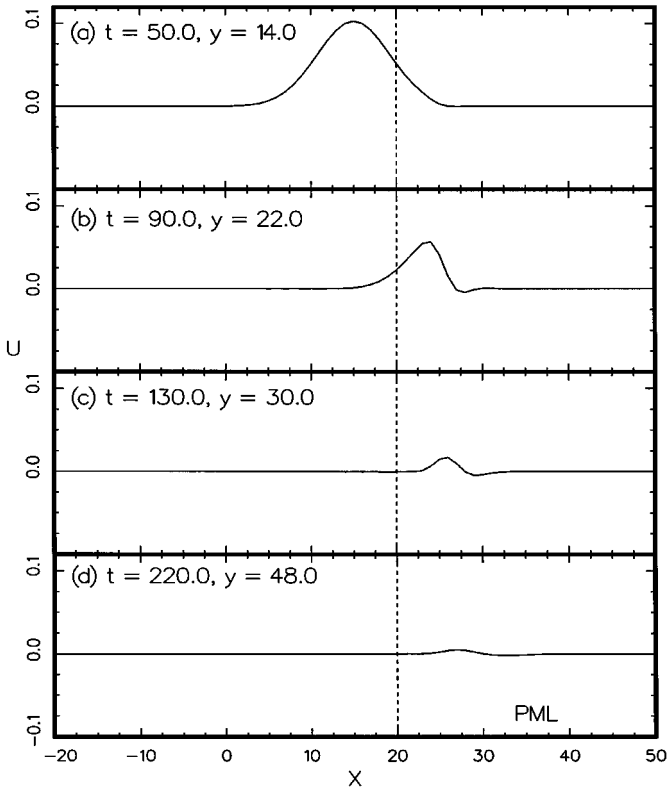


**FIG. 13.** Waveforms showing the damping of a vorticity wave packet as it is convected into a PML with artificial selective damping terms. $M_x = 0.3$, $M_y = 0.2$, $\sigma_m = 1.0$, $(R_\Delta^{-1})_{max} = 1.0$.

scale $\frac{R}{a_t}$, density scale $\rho_t$ (mean density at $r = R$), and pressure scale $\rho_t a_t^2$ will be used. The velocity components in the $(x, r, \phi)$ directions of a cylindrical coordinate system are denoted by $(u, v, w)$. For an inviscid compressible flow, the most general mean flow (designated by an overbar) is

$$\bar{u} = \bar{u}(r), \qquad \bar{v} = 0, \qquad \bar{w} = \bar{w}(r), \qquad \bar{\rho} = \bar{\rho}(r)$$

$$\bar{p} = -\int_r^1 \frac{\bar{\rho}\bar{w}^2}{r}\, dr + p_0. \tag{17}$$

Small amplitude disturbances superimposed on mean flow (17) are governed by the linearized Euler equations. They are

$$\frac{\partial \rho}{\partial t} + \frac{1}{r}\frac{\partial}{\partial r}(\bar{\rho} v r) + \frac{\bar{w}}{r}\frac{\partial \rho}{\partial \phi} + \bar{u}\frac{\partial \rho}{\partial x} + \bar{\rho}\left(\frac{1}{r}\frac{\partial w}{\partial \phi} + \frac{\partial u}{\partial x}\right) = 0 \tag{18a}$$

$$\bar{\rho}\left[\frac{\partial v}{\partial t} + \bar{u}\frac{\partial v}{\partial x} + \frac{\bar{w}}{r}\frac{\partial v}{\partial \phi} - \frac{2\bar{w}w}{r}\right] - \rho\frac{\bar{w}^2}{r} = -\frac{\partial p}{\partial r} \tag{18b}$$

$$\bar{\rho}\left[\frac{\partial w}{\partial t} + \bar{u}\frac{\partial w}{\partial x} + v\frac{d\bar{w}}{dr} + \frac{\bar{w}}{r}\frac{\partial w}{\partial \phi} + \frac{\bar{w}v}{r}\right] = -\frac{1}{r}\frac{\partial p}{\partial \phi} \tag{18c}$$

$$\bar{\rho}\left[\frac{\partial u}{\partial t}+\bar{u}\frac{\partial u}{\partial x}+v\frac{d\bar{u}}{dr}+\frac{\bar{w}}{r}\frac{\partial u}{\partial \phi}\right]=-\frac{\partial p}{\partial x} \tag{18d}$$

$$\frac{\partial p}{\partial t}+\bar{u}\frac{\partial p}{\partial x}+\frac{\bar{w}}{r}\frac{\partial p}{\partial \phi}+\frac{\bar{\rho}\bar{w}^2}{r}v+\gamma\bar{p}\left[\frac{1}{r}\frac{\partial vr}{\partial r}+\frac{1}{r}\frac{\partial w}{\partial \phi}+\frac{\partial u}{\partial x}\right]=0, \tag{18e}$$

where $\gamma$ is the ratio of specific heats. The boundary condition at the duct wall is

$$r=1, \qquad v=0. \tag{19}$$

Solutions of (18) and (19) representing propagating wave modes in the duct may be written in the form

$$\begin{bmatrix}\rho\\ u\\ v\\ w\\ p\end{bmatrix}=\mathrm{Re}\left\{\begin{bmatrix}\tilde{\rho}(r)\\ \tilde{u}(r)\\ \tilde{v}(r)\\ \tilde{w}(r)\\ \tilde{p}(r)\end{bmatrix}\exp[i(kx+m\phi-\omega t)]\right\}. \tag{20}$$

Substitution of (20) into (18) and (19) leads to the eigenvalue problem

$$\tilde{\rho}+\frac{i}{\omega r}\frac{d}{dr}(\bar{\rho}\tilde{v}r)-\frac{m\bar{w}}{\omega r}\tilde{\rho}-\frac{k\bar{u}}{\omega}\tilde{\rho}-\bar{\rho}\left(\frac{m}{\omega r}\tilde{w}+\frac{k}{\omega}\tilde{u}\right)=0 \tag{21a}$$

$$\bar{\rho}\left[\left(1-\frac{k}{\omega}\bar{u}-\frac{m\bar{w}}{\omega r}\right)\tilde{v}-i\frac{2\bar{w}\tilde{w}}{\omega r}\right]-\frac{i\tilde{\rho}\bar{w}^2}{\omega r}=-\frac{i}{\omega}\frac{d\tilde{p}}{dr} \tag{21b}$$

$$\bar{\rho}\left[\left(1-\frac{k}{\omega}\bar{u}-\frac{m\bar{w}}{\omega r}\right)\tilde{w}+\frac{i}{\omega}\tilde{v}\frac{d\bar{w}}{dr}+\frac{i\bar{w}}{\omega r}\tilde{v}\right]=\frac{m}{\omega r}\tilde{p} \tag{21c}$$

$$\bar{\rho}\left[\left(1-\frac{k}{\omega}\bar{u}-\frac{m\bar{w}}{\omega r}\right)\tilde{u}+\frac{i}{\omega}\tilde{v}\frac{d\bar{u}}{dr}\right]=\frac{k}{\omega}\tilde{p} \tag{21d}$$

$$\left(1-\frac{k\bar{u}}{\omega}-\frac{m\bar{w}}{\omega r}\right)\tilde{p}+\frac{i}{\omega}\frac{\bar{\rho}\bar{w}^2}{r}\tilde{v}+\gamma\bar{p}\left[\frac{i}{\omega r}\frac{d(\tilde{v}r)}{dr}-\frac{m}{\omega r}\tilde{w}-\frac{k}{\omega}\tilde{u}\right]=0 \tag{21e}$$

$$r=1, \qquad \tilde{v}=0. \tag{22}$$

For a given azimuthal mode number $m$ and frequency $\omega$, $k$ (the wavenumber) is the eigenvalue. Corresponding to an eigenvalue is an eigenvector $[\tilde{\rho}, \tilde{u}, \tilde{v}, \tilde{w}, \tilde{p}]$, which describes the radial profile of the wave mode.

### 4.1. *Perfectly Matched Condition in Ducted Flows*

Suppose a perfectly matched layer is to be set up as a termination boundary of a computation domain inside a duct. By splitting the variables, e.g., $\rho=\rho_1+\rho_2$, etc., in the standard manner, the PML equations corresponding to the linearized Euler equations ((18a)

to (18e)) are

$$\frac{\partial \rho_1}{\partial t} + \frac{1}{r}\frac{\partial}{\partial r}[\bar{\rho}(v_1 + v_2)r] + \frac{\bar{w}}{r}\frac{\partial(\rho_1 + \rho_2)}{\partial \phi} + \frac{\bar{\rho}}{r}\frac{\partial(w_1 + w_2)}{\partial \phi} = 0 \tag{23a}$$

$$\frac{\partial \rho_2}{\partial t} + \sigma \rho_2 + \bar{u}\frac{\partial(\rho_1 + \rho_2)}{\partial x} + \bar{\rho}\frac{\partial(u_1 + u_2)}{\partial x} = 0 \tag{23b}$$

$$\bar{\rho}\left[\frac{\partial v_1}{\partial t} + \frac{\bar{w}}{r}\frac{\partial(v_1 + v_2)}{\partial \phi} - \frac{2\bar{w}(w_1 + w_2)}{r}\right] - (\rho_1 + \rho_2)\frac{\bar{w}^2}{r} = -\frac{\partial}{\partial r}(p_1 + p_2) \tag{23c}$$

$$\bar{\rho}\left[\frac{\partial v_2}{\partial t} + \sigma v_2 + \bar{u}\frac{\partial(v_1 + v_2)}{\partial x}\right] = 0 \tag{23d}$$

$$\bar{\rho}\left[\frac{\partial w_1}{\partial t} + (v_1 + v_2)\frac{d\bar{w}}{dr} + \frac{\bar{w}}{r}\frac{\partial(w_1 + w_1)}{\partial \phi} + \frac{\bar{w}}{r}(v_1 + v_2)\right] = -\frac{1}{r}\frac{\partial(p_1 + p_2)}{\partial \phi} \tag{23e}$$

$$\bar{\rho}\left[\frac{\partial w_2}{\partial t} + \sigma w_2 + \bar{u}\frac{\partial(w_1 + w_2)}{\partial x}\right] = 0 \tag{23f}$$

$$\bar{\rho}\left[\frac{\partial u_1}{\partial t} + (v_1 + v_2)\frac{d\bar{u}}{dr} + \frac{\bar{w}}{r}\bar{u}\frac{\partial(u_1 + u_2)}{\partial \phi}\right] = 0 \tag{23g}$$

$$\bar{\rho}\left[\frac{\partial u_2}{\partial t} + \sigma u_2 + \bar{u}\frac{\partial(u_1 + u_2)}{\partial x}\right] = -\frac{\partial(p_1 + p_2)}{\partial x} \tag{23h}$$

$$\frac{\partial p_1}{\partial t} + \frac{\bar{w}}{r}\frac{\partial(p_1 + p_2)}{\partial \phi} + \frac{\bar{\rho}\bar{w}^2}{r}(v_1 + v_2) + \gamma\bar{p}\left[\frac{1}{r}\frac{\partial r(v_1 + v_2)}{\partial r} + \frac{1}{r}\frac{\partial(w_1 + w_2)}{\partial \phi}\right] = 0 \tag{23i}$$

$$\frac{\partial p_2}{\partial t} + \sigma p_2 + \bar{u}\frac{\partial(p_1 + p_2)}{\partial x} + \gamma\bar{p}\frac{\partial(u_1 + u_2)}{\partial x} = 0, \tag{23j}$$

where $\sigma$ is the damping coefficient in the PML. The boundary condition is

$$r = 1, \qquad v_1 + v_2 = 0. \tag{24}$$

In the PML, the duct modes are represented by solutions of the form (similar to (20))

$$\rho_1(r, \phi, x, t) = \mathrm{Re}\left[\hat{\rho}_1(r)e^{i(\kappa x + m\phi - \omega t)}\right], \tag{25}$$

etc., where $\kappa$ is the wavenumber. On substituting (25) into (23) and (24) and on defining

$$\begin{aligned} \hat{\rho} &= \hat{\rho}_1 + \hat{\rho}_2 \\ \hat{u} &= \hat{u}_1 + \hat{u}_2 \\ \hat{v} &= \hat{v}_1 + \hat{v}_2 \\ \hat{w} &= \hat{w}_1 + \hat{w}_2 \\ \hat{p} &= \hat{p}_1 + \hat{p}_2 \end{aligned} \tag{26}$$

it is straightforward to find that the duct modes in the PML are given by the solutions of the eigenvalue problem

$$\hat{\rho} + \frac{i}{\omega r}\frac{d}{dr}(\bar{\rho}\hat{v}r) - \frac{m\bar{w}}{\omega r}\hat{\rho} - \frac{\kappa\bar{u}}{\omega + i\sigma}\hat{\rho} - \bar{\rho}\left(\frac{m}{\omega r}\hat{w} + \frac{\kappa}{\omega + i\sigma}\hat{u}\right) = 0 \tag{27a}$$

$$\bar{\rho}\left[\left(1-\frac{\kappa}{\omega+i\sigma}\bar{u}-\frac{m\bar{w}}{\omega r}\right)\hat{v}-i\frac{2\bar{w}\hat{w}}{\omega r}\right]-\frac{i\hat{\rho}\bar{w}^2}{\omega r}=-\frac{i}{\omega}\frac{d\hat{p}}{dr} \tag{27b}$$

$$\bar{\rho}\left[\left(1-\frac{\kappa}{\omega+i\sigma}\bar{u}-\frac{m\bar{w}}{\omega r}\right)\hat{w}+\frac{i}{\omega}\hat{v}\frac{d\bar{w}}{dr}+\frac{i\bar{w}}{\omega r}\hat{v}\right]=\frac{m}{\omega r}\hat{p} \tag{27c}$$

$$\bar{\rho}\left[\left(1-\frac{\kappa}{\omega+i\sigma}\bar{u}-\frac{m\bar{w}}{\omega r}\right)\hat{u}+\frac{i}{\omega}\hat{v}\frac{d\bar{u}}{dr}\right]=\frac{\kappa}{\omega+i\sigma}\hat{p} \tag{27d}$$

$$\left(1-\frac{\kappa\bar{u}}{\omega+i\sigma}-\frac{m\bar{w}}{\omega r}\right)\hat{p}+\frac{i}{\omega}\frac{\bar{\rho}\bar{w}^2}{r}\hat{v}+\gamma\bar{p}\left[\frac{i}{\omega r}\frac{d(\hat{v}r)}{dr}-\frac{m}{\omega r}\hat{w}-\frac{\kappa}{\omega+i\sigma}\hat{u}\right]=0. \tag{27e}$$

The boundary condition is

$$r=1,\qquad \hat{v}=0. \tag{28}$$

The eigenvalue is $\kappa$. On comparing the eigenvalue problem (21) and (22) with the eigenvalue problem (27) and (28), it is immediately clear that they are the same if $\frac{k}{\omega}$ in (21) is replaced by $\frac{\kappa}{\omega+i\sigma}$. Thus the eigenvalues are related by

$$\kappa=k\left(1+\frac{i\sigma}{\omega}\right). \tag{29}$$

On the other hand, the eigenvectors are identical. The fact that the eigenvectors of a duct mode in the interior region of the computation domain is the same as that in the PML assures that there is perfect matching. That is, a propagating duct mode incident on the PML will be totally transmitted into the PML without reflection. If the mean flow is nonuniform, some of the duct modes may involve Kelvin–Helmholtz or other types of flow instability waves. However, the perfectly matched condition is still valid for these waves.

### 4.2. *The Case of Uniform Mean Flow*

From (25) and (29), the transmitted wave mode has the form

$$[\hat{\rho}(r),\hat{u}(r),\hat{v}(r),\hat{w}(r),\hat{p}(r)]e^{i[k(1+\frac{i\sigma}{\omega})x+m\phi-\omega t]}. \tag{30}$$

If the wave mode is nondispersive, then $\frac{k}{\omega}$, the inverse of the phase velocity, is positive for waves propagating in the $x$-direction and negative in the opposite direction. For these nondispersive waves, the transmitted waves are spatially damped, a condition needed by the PML if it is to serve as an absorbing boundary condition. However, inside a duct, the wave modes are dispersive. The direction of propagation is given by the group velocity $\frac{d\omega}{dk}$. We will now show that in the presence of a uniform mean flow there is a band of acoustic duct modes for which the group velocity and the phase velocity have opposite signs. Therefore, for this band of waves, the transmitted waves would grow spatially instead of being damped.

By eliminating all the other variables in favor of $\tilde{p}(r)$, it is straightforward to find, in the case of a uniform mean flow of Mach number $M$, (21) and (22) reduce to the following simple eigenvalue problem,

$$\frac{d^2\tilde{p}}{dr^2}+\frac{1}{r}\frac{d\tilde{p}}{dr}+\left[(\omega-Mk)^2-k^2-\frac{m^2}{r^2}\right]\tilde{p}=0 \tag{31}$$

$$r = 1, \qquad \frac{d\tilde{p}}{dr} = 0. \tag{32}$$

The eigenfunction is

$$\tilde{p} = J_m(\lambda_{mn} r), \tag{33}$$

where $J_m(\ )$ is the $m$th order Bessel function and $\lambda_{mn}$ is the $n$th root of

$$J'_m(\lambda_{mn}) = 0. \tag{34}$$

By substitution of (33) into (31), it is found that the dispersion relation or eigenvalue equation for the $(m, n)$th acoustic duct mode is

$$(\omega - Mk)^2 - k^2 = \lambda_{mn}^2. \tag{35}$$

The axial wavenumbers of the mode at frequency $\omega$ are given by the solution of (35). They are

$$k_{\pm} = \frac{-\omega M \pm \left[\omega^2 - (1 - M^2)\lambda_{mn}^2\right]^{\frac{1}{2}}}{(1 - M^2)}. \tag{36}$$

The group velocity of the duct mode may be determined by implicit differentiation of (35). This gives

$$\frac{d\omega}{dk} = \frac{\pm\left[\omega^2 - (1 - M^2)\lambda_{mn}^2\right]^{\frac{1}{2}}(1 - M^2)}{\omega \mp M\left[\omega^2 - (1 - M^2)\lambda_{mn}^2\right]^{\frac{1}{2}}}. \tag{37}$$

In (37), the upper sign corresponds to $k = k_+$ and the lower sign corresponds to $k = k_-$. For subsonic mean flow, clearly $\frac{d\omega}{dk} > 0$ for $k = k_+$ and $\frac{d\omega}{dk} < 0$ for $k = k_-$. Therefore, the downstream propagating waves have wavenumber given by $k = k_+$, while the upstream propagating waves have wavenumber equal to $k_-$.

From (37), it is easy to show that for $(1 - M^2)^{\frac{1}{2}}\lambda_{mn} < \omega < \lambda_{mn}$ the phase velocity $\frac{k_+}{\omega}$ is negative although the group velocity is positive. According to (29), for waves in this frequency band, the transmitted wave in the PML will amplify spatially. This renders the PML useless as an absorbing layer except for $M = 0$. In the absence of a mean flow normal to the PML $(M = 0)$, $k_+$ will not be negative by (36). Thus, the transmitted waves in the PML are evanescent. For this special condition, the PML can again be used as an absorbing boundary condition.

### 4.3. *Numerical Examples*

To demonstrate that a PML in a ducted environment actually supports a band of amplifying wave modes, a series of numerical simulations has been carried out. In the simulations, a uniform mesh with $\Delta x = \Delta r = 0.04$ covering the entire computation domain from $x = -6.0$ to $x = 12.0$ is used. The PML in the upstream direction begins at $x = -3.0$ and extends

to $x = -6.0$. In the downstream direction, the PML occupies the region from $x = 3.0$ to $x = 12.0$. The dimensionless damping constant (nondimensionalized by $\frac{a_\infty}{R}$) $\sigma$ is set equal to 25.0. The results of two simulations, one with a mean flow Mach number 0.4, the other two no mean flow, are reported below.

For convenience, only the axisymmetric duct modes are considered. The computation uses the 7-point stencil DRP scheme [13]. The acoustic disturbances in the computation domain are initiated by a pressure pulse located at $x = 0$ and $r = 0.5$. The initial condition is

$$t = 0, \qquad u = v = 0, \qquad p = \rho = \exp\left[-(ln\,2)\frac{(x^2 + (r - 0.5)^2)}{16}\right]. \tag{38}$$

Figure 14 shows the time evolution of the acoustic disturbance inside the computation domain at $M = 0.4$. Specifically, the pressure waveforms along the line $r = 0.38$ are shown at $t = 10$, 13, 15, and 16. As can be seen, once the pressure pulse is released, it spreads out and propagates upstream and downstream. Figure 14a indicates that at time $t = 10$ the front of the acoustic disturbance has just entered the PML in the downstream direction. There is no evidence of wave reflection at the interface between the PML and the interior computation domain. The transmitted wave grows spatially as shown in Fig. 14b. The amplitude of the transmitted wave increases steadily as they propagate across the PML. This is shown in

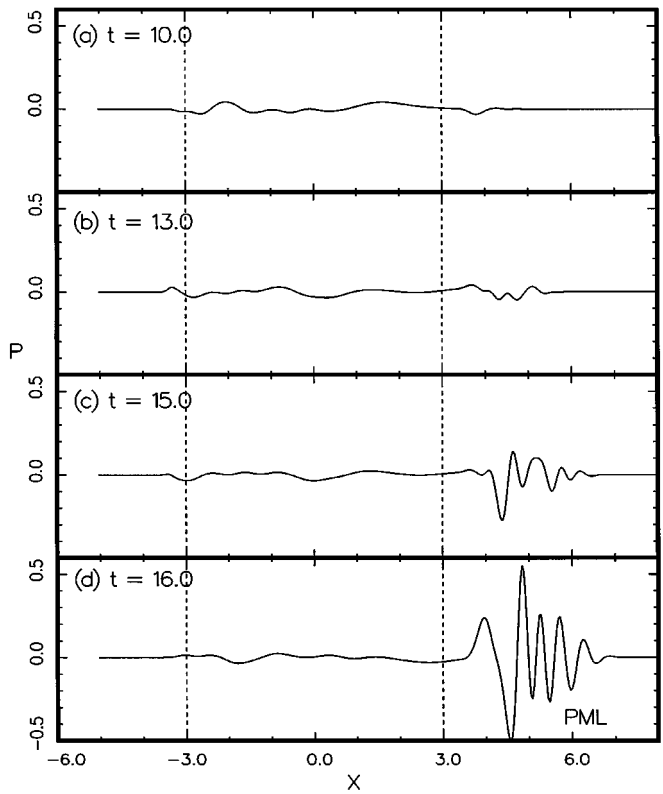


**FIG. 14.** Pressure waveforms along the line $r = 0.38$ of a circular duct with uniform mean flow at Mach 0.4 showing the excitation and growth of the unstable solution in the PML by an acoustic pulse. $\Delta x = \Delta r = \frac{R}{25}$, $\sigma_m = 25.0$.

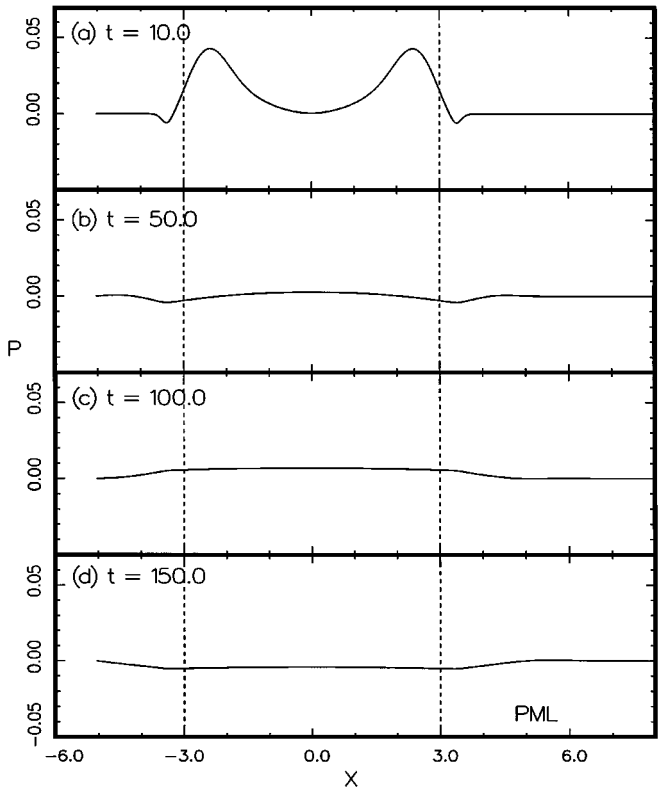


**FIG. 15.** Pressure waveforms along the line $r = 0.38$ of a circular duct without mean flow showing the damping of an acoustic pulse in the PML. $\Delta x = \Delta r = \frac{R}{25}$, $\sigma_m = 25.0$.

Figs. 14c and 14d. When the amplified waves reach the outermost boundary of the PML, large amplitude spurious waves are reflected back. This quickly contaminates the entire computation domain.

Figure 15 shows the same simulation except that there is no mean flow. In the absence of a mean flow, the PML acts as an absorbing layer. Figure 15a shows the entry of the acoustic pulse into the downstream PML. Figures 15b to 15d show the damping of the acoustic pulse in time in the PML. The slowest components to decay are the long waves. This is in agreement with the analysis of the previous section.

## 5. CONCLUDING REMARKS

In this paper, we have shown that the application of PML as an absorbing boundary condition for the linearized Euler equations works well as long as there is no mean flow in the direction normal to the layer. For open domain problems, the PML equations, in the presence of a subsonic mean flow normal to the layer, support unstable solutions. The growth rate of the unstable solutions is, however, not large. These unstable solutions can, generally, be suppressed by the addition of artificial selective damping. In the case of a ducted environment, we find that because of the highly dispersive nature of the duct modes, a band of the transmitted waves in the PML amplifies instead of being damped. This band consists of long waves so that they are not readily suppressed by the inclusion of artificial

selective damping. This seemingly renders the PML totally ineffective as an absorbing boundary condition.

One of the important advantages of using an absorbing boundary condition instead of other numerical boundary treatments is that the boundary of the computation domain may be put much closer to the source of disturbances. In this way, a smaller computation domain may be used in a numerical simulation. For open domains, such an absorbing boundary condition can be developed by the use of PML with artificial selective damping terms. Unfortunately, the same is not possible for internal ducted flow. An effective numerical anechoic termination for ducted domains has yet to be developed.

## ACKNOWLEDGMENT

This work was supported by NASA Langley Research Grant NAG 1-1776.

## REFERENCES

1. J. P. Berenger, A perfectly matched layer for the absorption of electromagnetic waves, *J. Comput. Phys.* **114**, 185 (1994).
2. J. P. Berenger, Three dimensional perfectly matched layer for the absorption of electromagnetic waves, *J. Comput. Phys.* **127**, 363 (1996).
3. F. D. Hastings, J. B. Schneider, and S. L. Broschat, Application of the perfectly matched layer (PML) absorbing boundary condition to elastic wave propagation, *J. Acoust. Soc. Amer.* **100**, 3061 (1996).
4. F. Q. Hu, On absorbing boundary conditions for linearized Euler equations by a perfectly matched layer, *J. Comput. Phys.* **129**, 201 (1996).
5. F. Q. Hu, On perfectly matched layer as an absorbing boundary condition, AIAA paper 96-1664, 1996.
6. M. Hayder, F. Q. Hu, and Y. M. Hussaini, Toward perfectly matched boundary conditions for Euler equations, AIAA paper 97-2075, 1997.
7. F. Q. Hu and J. L. Manthey, Application of PML absorbing boundary conditions to the benchmark problems of computational aeroacoustics, in *Proc. Second Comput. Aeroacoustics Workshop on Benchmark Problems* (NASA CP-3352, 1997), p. 119.
8. P. M. Morse and K. U. Ingard, *Theoretical Acoustics* (McGraw–Hill, New York, 1968).
9. W. Eversman, Theoretical models for duct acoustic propagation and radiation, in *Aeroacoustics of Flight Vehicles: Theory and Practice* (NASA RP-1258, 1991), Vol. 2, Chap. 13, p. 101.
10. C. K. W. Tam, Advances in numerical boundary conditions for computational aeroacoustics, *J. Comput. Acoustics*, in press.
11. S. Abarbanel and D. Gottlieb, A mathematical analysis of the PML method, *J. Comput. Phys.* **134**, 357 (1997).
12. C. K. W. Tam, J. C. Webb, and Z. Dong, A study of the short wave components in computational acoustics, *J. Comput. Acoustics* **1**, 1 (1993).
13. C. K. W. Tam and J. C. Webb, Dispersion-relation-preserving finite difference schemes for computational acoustics, *J. Comput. Phys.* **107**, 262 (1993).
14. C. K. W. Tam, Computational aeroacoustics: Issues and methods, *AIAA J.* **33**, 1788 (1995).